Received: 29 May 2016 | Revised: 12 September 2017 | Accepted: 13 September 2017

DOI: 10.1002/we.2147

WILEY

RESEARCH ARTICLE

An experimental investigation on the wake interferences among wind turbines sited in aligned and staggered wind farms

Wei Tian[1,2] | Ahmet Ozbay[2] | Hui Hu[2]

[1] School of Aeronautics and Astronautics, Shanghai Jiao Tong University, Shanghai 200240, China

[2] Department of Aerospace Engineering, Iowa State University, Ames, IA 50010, USA

Correspondence
Hui Hu, Department of Aerospace Engineering, Iowa State University, Ames, IA 50010, USA.
Email: huhui@iastate.edu

Funding information
National Science Foundation (NSF), Grant/Award Number: CBET-1133751 CBET-1438099; Shanghai Natural Science Foundation, Grant/Award Number: 16ZR1417600; National Key Technology Support Program of China, Grant/Award Number: 2015BAA06B04; Iowa Energy Center, Grant/Award Number: 14-008-OG

Abstract

An experimental investigation was conducted for a better understanding of the wake interferences among wind turbines sited in wind farms with different turbine layout designs. Two different types of inflows were generated in an atmospheric boundary layer wind tunnel to simulate the different incoming surface winds over typical onshore and offshore wind farms. In addition to quantifying the power outputs and dynamic wind loads acting on the model turbines, the characteristics of the wake flows inside the wind farms were also examined quantitatively. After adding turbines staggered between the first 2 rows of an aligned wind farm to increase the turbine number density in the wind farm, the added staggered turbines did not show a significant effect on the aeromechanical performance of the downstream turbines for the offshore case. However, for the onshore case, while the upstream staggered turbines have a beneficial effect on the power outputs of the downstream turbines, the fatigue loads acting on the downstream turbines were also found to increase considerably due to the wake effects induced by the upstream turbines. With the same turbine number density and same inflow characteristics, the wind turbines were found to be able to generate much more power when they are arranged in a staggered layout than those in an aligned layout. In addition, the characteristics of the dynamic wind loads acting on the wind turbines sited in the aligned layout, including the fluctuation amplitudes and power spectrum, were found to be significantly different from those with staggered layout.

KEYWORDS

atmospheric boundary layer, wake interference, wind farm layout optimization, wind tunnel testing, wind turbine aerodynamics

1 | INTRODUCTION

The development of large wind farms and improvement of wind farm's reliability and effectiveness are urgently required for wind energy production. Large wind farms necessitate the organization of multiple wind turbines into large arrays, leading to concerns about wind farm efficiency. It has been reported that wind turbines operating in a large wind farm may suffer up to 30% power loss[1-3] and up to 80% more fatigue loads.[4] These significant power losses and enhanced fatigue loads were found to be caused by the effects of wake interferences among turbines installed in large arrays.

A good understanding of the turbine wake characteristics is very important for evaluating the effects of wake interferences among multiple wind turbines to explore paradigms for the optimal design of turbine array spacing and layout in wind farms. To investigate wind turbine wake aerodynamics, both numerical and experimental studies have been conducted in which an isolated wind turbine is considered as the first step toward a better understanding of wake interference among multiple wind turbines. For example, Wu and Porté-Agel[5] simulated the wake behind a wind turbine placed in a neutrally stratified boundary layer by using large-eddy simulation (LES) coupled with wind turbine models. Hu et al[6] and Zhang et al[7] experimentally studied turbulent vortex structures in the wakes of isolated wind turbine models placed in atmospheric boundary layer (ABL) winds. A subject of special concern is the effect of inflow turbulence on the vortex structure and evolution of wind turbine wakes. Chamorro and Porté-Agel[8] carried out experiments in the wake of a wind turbine model sited in a

boundary layer wind tunnel with rough and smooth surfaces to investigate the influence of atmospheric turbulence intensity on the turbine wake characteristics. They showed that the effect of inflow turbulence is not negligible even at a downwind distance of 15*D* (where *D* is the rotor diameter). Wu and Porté-Agel[9] performed an LES study to investigate the characteristics of turbine wakes over homogeneous flat surfaces with 4 different roughness lengths of neutrally stratified ABL winds. They found that different inflow turbulence levels lead to distinct effects on the wake characteristics, including mean velocity deficit, turbulence intensity, and turbulent shear stress. Chu and Chiang[10] experimentally investigated the effects of ambient turbulence on the turbine wake flows and power production of a model wind turbine. Their work indicated that, due to the enhanced mixing associated with the grid-generated highly turbulent flow, velocity deficits were consistently found to be smaller than that in low turbulence flow. More recently, an experimental study performed by Tian et al[11] reported the effect of inflow turbulence on the characteristics of turbine near wakes and dynamic wind loading acting on a model turbine in an ABL wind tunnel.

In comparison with those in the wake behind an isolated wind turbine, the flow characteristics in a wind farm would be influenced by more complicated factors, including the effects of the local topography, the coexistence of multiple superimposed wakes, stratified turbulent winds, and elevated turbulence levels. Sescu and Meneveau[12] numerically studied the effects of atmospheric thermal stability on the asymptotic behavior of very large wind farms. Wu and Porté-Agel[13] proposed an LES framework to study multiple wake flows and associated power losses in a large wind farm. The predicted power outputs agree well with onsite measurement data obtained from the Horns Rev wind farm. Yang et al[14] developed a numerical approach to simulate the interaction of terrain-induced turbulence with wind turbines sited in a large wind farm over complex terrain. Recently, a LES study performed by Cortina et al[15] indicated that the recovery of mean kinetic energy around a characteristic wind turbine in a very large wind farm is dominated by the vertical flux. While a number of numerical and theoretical investigations have been performed for the development of wake models to predict flow characteristics inside wind farms,[12-16] numerous onsite and wind tunnel experiments have also been conducted to evaluate the characteristics of turbulent flows and wake interferences among multiple turbines. In particular, wind tunnels have been widely used for wind farm investigations due to their ability to produce well-controlled flow conditions. Cal et al[17] performed detailed particle image velocimetry measurements in a 3 × 3 wind turbine array to investigate the averaged flow structures within the turbine array. Chamorro and Porté-Agel[18] experimentally studied turbulent flow structures inside and above a model wind farm with a 10 × 3 array of wind turbine models aligned in the incoming flow direction. Chamorro et al[19] investigated the flow characteristics around a perfectly staggered model wind farm and found that, in comparison with an aligned layout with similar turbine spacing, the staggered layout is more efficient in promoting kinetic energy transportation by entraining background flows into the turbine wakes. Subsequently, a direct comparison study of the flow within and over aligned and staggered wind farms was performed by Markfort et al[20] and found that the staggered layout would absorb momentum more efficiently than the aligned layout, leading to a greater overall power generation potential.

The effects of inflow turbulence on wind farm performance can be deduced based on the comparisons of the turbine power measurements in offshore wind farms with those in onshore wind farms. Barthelmie et al[21] reported that wake-induced power losses in offshore wind farms appear much larger than predicted a priori. It is likely due to low atmospheric turbulence that impedes wake recovery and reduces the power outputs from downstream turbines.[22] However, according to Barthelmie et al,[23] data analysis of onshore wind farms does not indicate as large a "deep array effect" as has been observed in offshore wind farms. They suggest that this finding may be a product of higher ambient turbulence levels and wind farm design for onshore wind farms (ie, onshore wind farms are more frequently arranged as irregular arrays). Hansen et al[24] also indicated that the power losses within an offshore (Horns Rev) wind farm are strongly related to the atmospheric turbulence levels. While the power production performance of a wind farm has been found to be highly related to the turbulent flow characteristics inside the wind farm, the effects of the incoming turbulent flow characteristics on the turbine wake interactions within the wind farms with different layouts are still not fully understood. Much work is still needed to elucidate the underlying physics and to exploit/optimize design paradigms for better power production performance and durability of wind turbines operating in wind farm settings.

While most of the previous wind tunnel studies focused on quantifying the turbulent flow characteristics over wind farms, the aeromechanical performances, eg, power outputs and dynamic wind loads, of wind turbines sited inside wind farms have been less studied. Adaramola and Krogstad[3] experimentally measured the performance of a model wind turbine operating in the wake of another turbine, considering the turbine spacing, blade pitch angle, and yaw angle of the upstream turbine. The power output characteristics of a 3-turbine array were measured by Annoni et al[25] to analyze the effect of individual turbine control on wind farm dynamics. Theunissen et al[26] performed a systematic study on turbine wake characteristics and variations in power generation with turbine layout for an 80 turbine wind farm. More recently, Bossuyt et al[27] conducted wind tunnel experiments to study the unsteady loading and spatial-temporal characteristics of power outputs of a wind farm model represented by using 100 porous disk models. The spatial-temporal characteristics of power outputs were used to examine the cross correlation of the wind farm power outputs in both aligned and staggered turbine layouts. Furthermore, Bossuyt et al[28] also indicated that the frequency spectrum of the aggregate power output from a wind farm would depend on both the wind farm layout and the turbulence properties of the incoming surface winds.

In this paper, an experimental study was conducted to explore the effects of the characteristics of incoming turbulent flows on the aeromechanical performances of wind turbines placed in either typical offshore or onshore wind farms with different turbine layouts. The experimental study was performed in a large-scale ABL wind tunnel. Two different types of ABL winds with distinct mean and turbulence characteristics were generated in the wind tunnel to simulate the different incoming surface winds over typical onshore and offshore wind farms.

An array of wind turbine models was mounted inside the ABL winds to form a small wind farm. During the experiments, the aeromechanic performances of the wind turbines, including power outputs and dynamic wind loads, were measured as they were arranged in either staggered or aligned layout. The turbulent flows over the wind farms in either aligned or staggered layouts were also measured quantitatively. The measured power outputs and dynamic wind loads were correlated with detailed flow field measurements to elucidate the underlying physics and to exploit/optimize wind farm design paradigms for higher power production and better durability of wind turbines operating in onshore or offshore wind farms.

2 | EXPERIMENTAL SETUP AND PROCEDURE

2.1 | Atmospheric boundary layer wind tunnel

The experimental study was conducted in a large-scale ABL wind tunnel available at Iowa State University. The test section of the ABL wind tunnel is 20 m long, 2.4 m wide, and 2.3 m high. For the present study, triangular spike structures and wooden block arrays with different size and array spacing were mounted on the wind tunnel floor upstream of the tested wind turbine models to generate 2 different ABL winds with distinct mean and turbulence characteristics (ie, 2 different inflows). This allowed us to simulate the surface winds over typical onshore and offshore wind farms in the ABL wind tunnel to evaluate the effects of the flow characteristics of the incoming ABL winds on the wake interferences among the wind turbines in either onshore or offshore wind farms. Further information about the settings of the spikes and wooden block arrays to generate ABL winds is available in Tian et al.[11] The simulated ABL winds have well-developed boundary layers over the area where the model wind farms were placed. The ceiling of the test section of the ABL wind tunnel can be adjusted to ensure 0 pressure gradients along the flow direction for the simulated ABL winds.

It is well known that the velocity profile of a typical ABL flow over a flat surface can usually be described with a logarithmic law, which can be expressed as

$$u(z) = \frac{u_*}{\kappa} \ln\left(\frac{z}{z_0}\right) \tag{1}$$

where u_* is the friction velocity, κ is the von Karman constant (≈0.4), and z_0 is the surface roughness length.

Figure 1 gives the measured mean velocity profiles for the 2 types of inflows generated in the ABL wind tunnel for the present study. The horizontal axis in the figure represents nondimensional mean velocity u/U_{Hub}, where U_{Hub} is the reference velocity at the wind turbine hub height (H). During the experiments, this reference velocity was kept as a constant (ie, U_{Hub} = 5.0 m/s) for both inflow cases. By fitting logarithmic profile to the measured velocity profiles, the parameters u_* and z_0 can be obtained. For the type 1 inflow case, the surface roughness length and friction velocity were found to be z_0 = 0.01mm and u_* = 0.20m/s, which can be used to represent the boundary layer over offshore (open sea) terrain according to the Australian Standard.[29] For the type 2 inflow case, the fitted friction velocity and surface roughness length were found to be u_* = 0.30m/s and z_0 = 0.30mm. As described in the Australian Standard,[29] this surface roughness length is representative of open terrain or grassland containing a small amount of scattered obstacles with heights approximately 1.5 to 10 m.

The turbulence intensity profile for the type 1 inflow is given in Figure 2A, which shows that the turbulence intensities in the turbine rotor region are approximately 10%, ie, within the range of the field measurement results obtained by Hansen et al[24] for typical offshore wind farms. Here, the turbulence intensity is calculated by $I_u = \sigma_u/U_{local}$, where σ_u is the root-mean-square value of the streamwise velocity fluctuations and U_{local} is the mean velocity at the measurement point. While offshore wind farms usually have relatively low turbulence levels, wind turbines sited

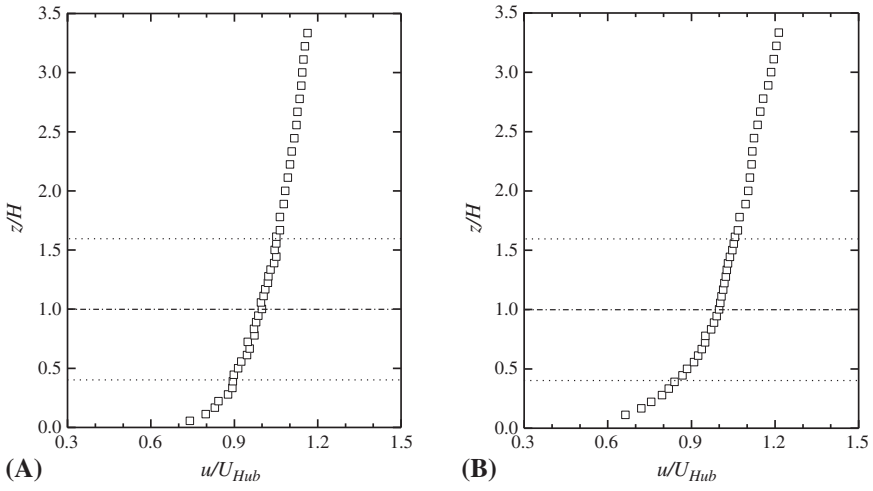

FIGURE 1 Measured time-averaged velocity profiles for the 2 types of incoming boundary layer flows generated in the atmospheric boundary layer (ABL) wind tunnel. A, Type 1 inflow; B, type 2 inflow (the 2 dotted lines represent the top and bottom tip heights of the wind turbine rotor; the dash-dotted line represents the turbine hub height)

in onshore wind farms would experience surface winds with much higher turbulence levels due to the effects of a number of factors, such as terrain topography, surface roughness, and thermal stratification. Figure 2B shows the measured turbulence intensity profile for the type 2 inflow. It can be seen that the magnitudes of the turbulence intensities in the turbine rotor region are almost twice as those of the type 1 inflow case.

2.2 | Wind turbine and wind farm models

The turbine models used in the present study are typical horizontal axial wind turbines, and each turbine has 3 ERS-100 rotor blades. Geometrical details about the ERS-100 rotor blades can be found in Locke and Valencia[30] and Somers.[31] The diameter of the turbine rotors is 280 mm, and the hub height to the wind turbines is 225 mm. Further information about the scaled turbine models is available in Tian et al[11] and Ozbay et al.[32] Because the ratio of the swept area of the turbine rotor to the cross-sectional area of the ABL tunnel is 1:110, the blockage effects of the turbine models on the wind tunnel experimental results can be neglected.

Figure 3 shows schematically the 3 wind farm layouts to be compared in the present study. The spanwise distance between wind turbine models was held as constant at 3*D* (*D* is the rotor diameter) for all the 3 wind farm layouts. As revealed in Figure 3A, 6 wind turbine models were arranged as an aligned layout in a 2 × 3 array with 6*D* spacing in streamwise direction, which is referred as the 6*D*-aligned layout in the present study. As shown in Figure 3B, 2 turbine models were added in the middle of the 6*D*-aligned layout with a staggered arrangement, which is called as 3*D*-staggered layout. It should be noted that the 3*D*-staggered and 6*D*-aligned layouts have the same streamwise spacing between the aligned turbines (6*D*). By comparing the measurement results with the wind farm layouts as shown in Figure 3A and B, the effects of the staggered upstream turbines on the aerodynamic performances of the downstream wind turbines can be evaluated to improve our understanding about the turbine wake interferences in staggered wind farms. As shown in Figure 3C, 3*D*-alinged layout refers the case with wind turbines being organized in an aligned layout of a 3 × 3 array with 3*D* streamwise spacing. It will be compared with the 3*D*-staggered layout case, as both the cases having the same streamwise and spanwise turbine spacing. It should also be noted that, while the 3*D*-staggered layout case shown in Figure 3B has only 8 wind turbines, the 3*D*-alinged layout case shown in Figure 3C has 9 turbines in the interrogation window. During the experiments, the power outputs and the dynamic wind loads acting on the wind turbines sited at the central position of the last row for different wind farm layouts (ie, as shown in the ellipses) are measured for the comparative study.

In addition to measuring the power outputs and the dynamic wind loads acting on the wind turbine models, the flow characteristics of the wind farm with different layouts were also examined in the present study. As shown in Figure 3D to F, the downstream wind turbines (ie, the turbines sited in the ellipses in Figure 3A-C) were removed before the flow measurements were performed. Therefore, the measured flow characteristics would reveal the incoming flow conditions for the wind turbines sited at the central position of the farm's last row. It should be noted that, in addition to the flow measurements along the vertical direction along the center lines (ie, at $y = 0$) of the 3 compared wind farm layouts, flow measurements were also carried out along the spanwise direction at turbine hub height (H) over a range of $y = -1.5D$ to $1.5D$.

2.3 | Measurement systems

In the present study, a Cobra Probe anemometry system (Turbulent Flow Instrumentation Pty Ltd) was used to measure the turbulent flow characteristics over the wind farms with different layouts. The measurement range of the anemometry system is 2 to 100 m/s with the accuracy level of 0.50%. By using the Cobra Probe, all 3 components of the velocity vector can be measured instantaneously. The time-averaged velocity and turbulent kinetic energy can also be calculated after obtaining the instantaneous measurement data. For the measurement results given in the present study, the sampling rate of the instantaneous velocity vector was set to be 1250 Hz with a measurement period of 60 seconds at each point of interest.

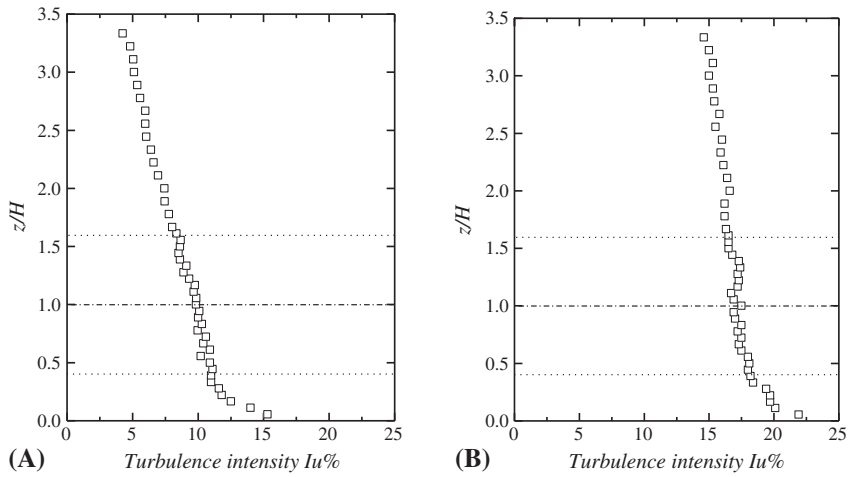

FIGURE 2 Measured turbulence intensity profiles for the 2 types of incoming boundary layer flows generated in the atmospheric boundary layer (ABL) wind tunnel. A, Type 1 inflow; B, type 2 inflow

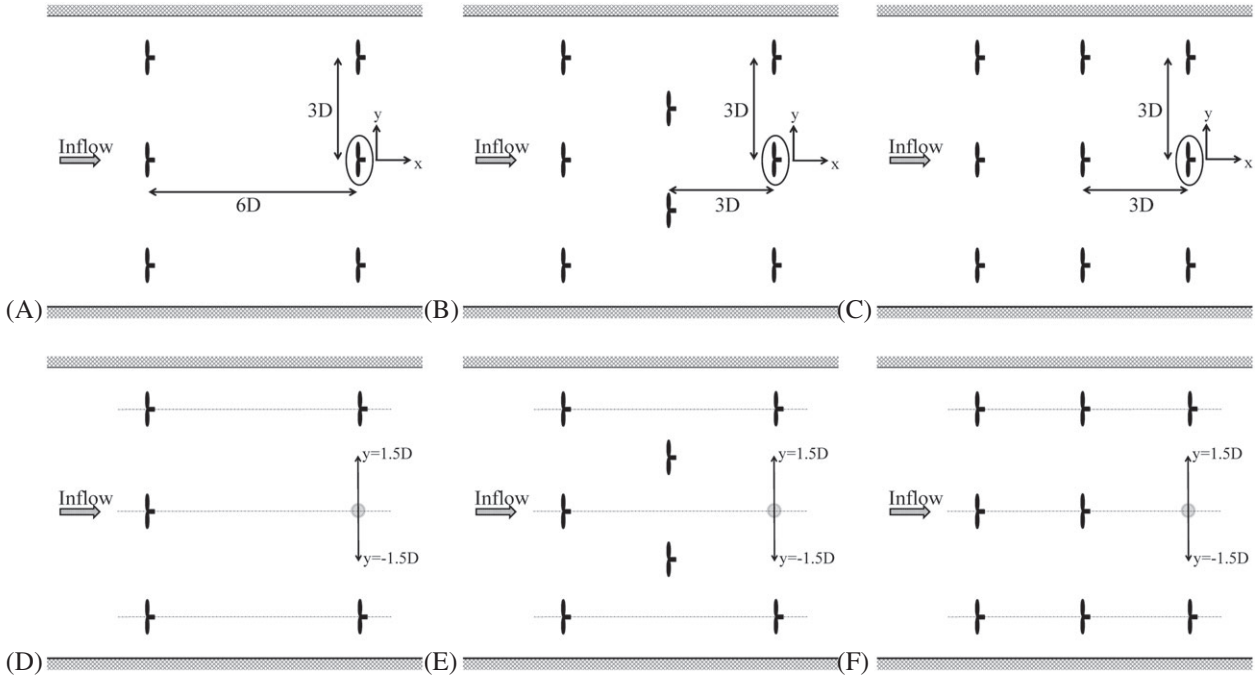

FIGURE 3 Schematic diagrams of the compared wind farm layouts and the selected locations for the flow measurements. A, 6*D*-aligned layout; B, 3*D*-staggered layout; C, 3*D*-aligned layout; D, measurement location for the 6*D*-aligned layout; E, measurement location for the 3*D*-staggered layout; F, measurement location for the 3*D*-aligned layout

A high-sensitivity load cell (JR3, model 30E12A-I40) was used to measure the dynamic wind loads acting on the turbine models. The JR3 load cell, which can provide instantaneous measurements of the forces and moment about all 3 axes, was mounted at the base of the model wind turbine. The standard load rating of the JR3 load cell is 40*N* for aerodynamic forces and 5*N* m for moments. In the present study, the coefficients of the force along the *x*-axis (ie, thrust force, *T*), the moment along the *y*-axis (ie, bending moment, M_y), and the force along the *y*-axis (ie, lateral force, F_y) were calculated as $C_T = T/(0.5\rho U_{\text{Hub}}{}^2\pi R^2)$, $CM_y = M_y/(0.5\rho U_{\text{Hub}}{}^2\pi R^2 H)$, and $C_y = F_y/(0.5\rho U_{\text{Hub}}{}^2\pi R^2)$, where ρ is the air density, H is the turbine hub height, and R is the radius of the model wind turbine rotor. During the experiments, the wind load data were sampled at a rate of 1000 Hz with a measurement period of 60 seconds.

In addition to measuring the wind loads, the power outputs generated by the turbine models were also measured by using the method developed by Kang and Meneveau.[33] As indicated by Kang and Meneveau,[33] a direct current (DC) generator attached to the turbine rotor was placed in the turbine nacelle and supported by a ball bearing system. During operation of the turbine model, the rotation of the DC generator was prevented by a strain-gauge-instrumented bronze plate via a light pressing rod attached to the rear of the DC generator. The torque of the rotating turbine rotor blades was obtained by measuring the bending moment of the deflected plate. During the experiments, a similar torque sensor was used to measure the torque of the turbine rotor blades. A Monarch tachometer was used to measure the rotational frequency of the wind turbine. Based on the measured torque T and the turbine rotational frequency Ω, the power coefficient of the wind turbine model was calculated as $C_p = T\Omega/(0.5\rho U_{\text{Hub}}{}^3\pi R^2)$. In the present study, the power coefficients of the tested turbine models were found to be $C_p = 0.15 - 0.3$. According to the uncertainty in the torque calibration and the uncertainty in reading the frequency from the tachometer, the relative uncertainty level for the power measurements was estimated to be approximately 6.0%.

In the present study, the turbine rotation frequency was changed by applying different electric loads to the DC generator placed inside the turbine nacelle. For each test case, a series of tip-speed ratio (TSR) values were adjusted to test the power output of the model wind turbine. The TSR value corresponding to the maximum power output was defined as the optimal TSR. The dynamic wind loads acting on the wind turbine model were measured under the optimal TSR.

3 | EXPERIMENTAL RESULTS AND DISCUSSIONS

3.1 | Wake characteristics in aligned and staggered wind farms

3.1.1 | Mean velocity

Figure 4 gives the measured time-averaged flow velocity profiles along the vertical direction at the selected positions in the 3 compared farms with different turbine layouts. The mean velocity of the undisturbed inflow is also given in the plot for comparison. A significant effect of the

inflow characteristics on the evolution of the wake flows inside the wind farms can be observed from the measurement results given Figure 4. The streamwise velocity deficits in the turbine wakes for the offshore farm cases were found to be much greater than those of the onshore cases for all the 3 compared farm layouts. Taking the 6*D*-aligned layout as an example, the streamwise velocity deficit at hub height was found to be approximately 16% for the offshore case (ie, the test case with the type 1 inflow), which is more than twice that for the onshore case (ie, the test case with the type 1 inflow). An obvious reduction in the streamwise flow velocities in the turbine wake above the top turbine tip height can also be seen from the measurements given in Figure 4. This is believed to be a consequence of the wake expansion behind and below the upstream wind turbines. For the 6*D*-aligned and 3*D*-staggered layout cases, the wake expansion was found to reach a height of z/H = 2.1 for the onshore wind farm case, which is only a little higher than that of the offshore case. In the present study, the wake expansion region is determined by the criterion that the difference in the mean velocity between the incoming flow and the wake flow is higher than 0.05 m/s (ie, 1.0% of the hub velocity). However, for the 3*D*-aligned layout cases, the wake expansion for the onshore case was found to reach a height of z/H = 3.1, which is much greater than that of the offshore case (ie, at z/H = 2.0). Such a significant difference is believed to be mainly caused by the closer turbine spacing and the presence of one more upstream turbine along the streamwise direction, as well as the high turbulence levels for the onshore case, which would promote the entrainment of more high-speed flow from above into the low momentum wakes between the wind turbines.

Figure 5 shows the measured mean velocity profiles at the turbine hub height along the spanwise direction inside the wind farms. It can be observed that the velocity profiles for the 3 compared turbine layouts were all found to be symmetric, corresponding to the rather uniform inflow velocity profiles. As shown in Figure 5A, the velocity profiles for all the 3 compared cases were found to fit well to a Gaussian distribution. The maximum velocity deficits appearing in the middle of the rotor plane for the 6*D*-aligned and 3*D*-staggered layout cases were found to be approximately 16%. For the 3*D*-aligned layout case, due to the much closer turbine spacing and presence of 1 more upstream turbine along the flow streamline to block the incoming flow, the maximum velocity deficit was found to reach 35%, which is more than twice that of the 6*D*-aligned and 3*D*-staggered layout cases.

For onshore wind farms, the measured velocity profile for the 6*D*-aligned layout case reveals that the wake expansion in the spanwise direction reaches $y = -1.5D$ to $1.5D$, which is much wider than that of the offshore farm case ($y = -0.8D$ to $0.8D$). Because a wider turbine wake region would indicate more areas for high momentum flows from outside to mix and "recharge" the low momentum turbine wake flows, the recovery rate of the turbine wake flows for the onshore farm case was found to be much faster than that of the offshore case. As shown in Figure 5B, the maximum velocity deficits in the middle of the turbine rotor plane for the 6*D*-aligned and 3*D*-staggered layout cases were found to be only approximately 4%, which are significantly lower than those of the offshore cases (ie, approximately 16%). Furthermore, as revealed clearly in Figure 5B, due to the much more intensive turbulence mixing in the turbine wakes for the onshore case, the turbine wake flows for the cases of 6*D*-aligned and 3*D*-staggered layouts were found to approach almost uniform flow in the region of $y = -0.5D$ to $0.5D$ (ie, within the rotor region for the downstream turbine), which is very different from those of the offshore case (ie, fitted well by Gaussian curves) shown in Figure 5A.

Based on the measured flow velocity profiles given in Figure 5, local flow acceleration can also been observed for the case with 3*D*-staggered layout, which is believed to be caused by the lateral offset of the turbines in the second row of the wind farm. As described in Chamorro et al,[19] Markfort et al,[20] and Ammara et al,[34] such behavior could be attributed to the Venturi effect induced by the lateral offset of the wind turbines in the staggered rows. Within the rotor region of the central turbine sited in the last row (ie, $y = -0.5D$ to $0.5D$), the flow velocities in the farms for the 3*D*-staggered layout case were found to be always slightly higher than those of the 6*D*-aligned layout case. Thus, even though the turbine number density for the 3*D*-staggered layout case is higher than that of the 6*D*-aligned layout case, the downstream turbines in the wind farm with 3*D*-staggered layout still can extract more energy from the same incoming flow than those in the wind farm with 6*D*-aligned layout due to the Venturi effect.

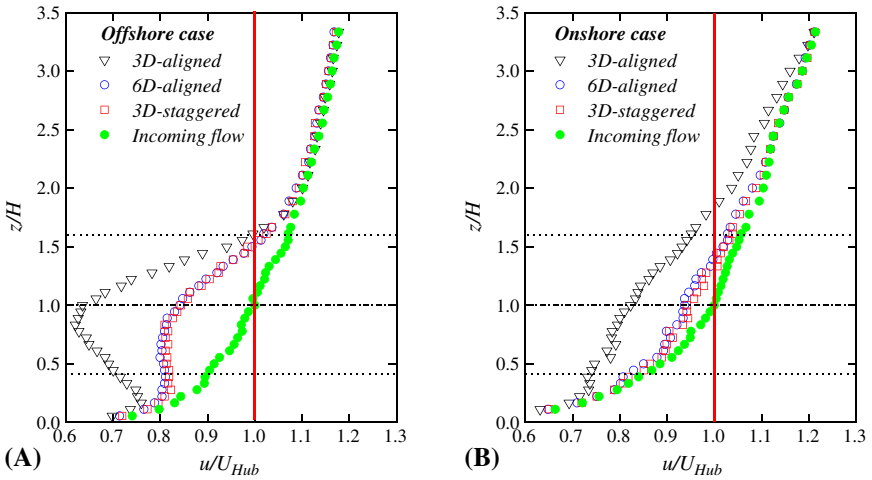

FIGURE 4 Measured velocity profiles along vertical direction for the farms with different turbine layouts. A, Offshore case; B, onshore case [Colour figure can be viewed at wileyonlinelibrary.com]

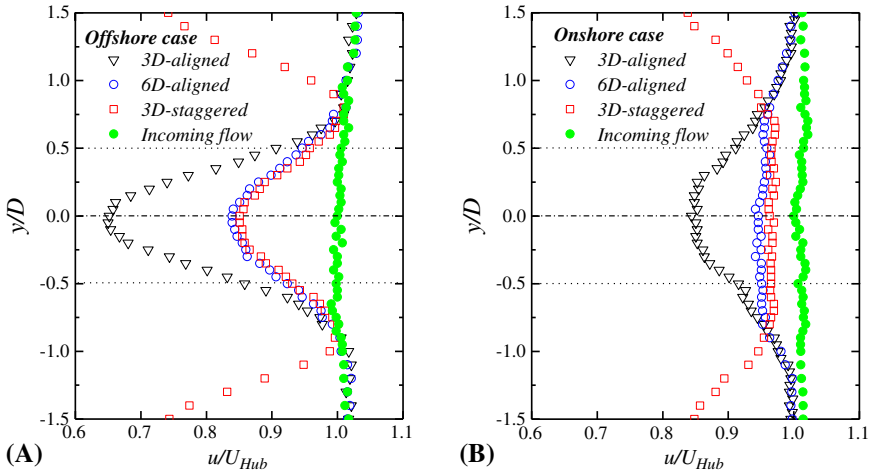

FIGURE 5 Measured velocity profiles along spanwise direction for the farms with different turbine layouts. A, Offshore case; B, onshore case [Colour figure can be viewed at wileyonlinelibrary.com]

3.1.2 | Turbulent kinetic energy

Figure 6 shows the vertical profiles of measured TKE for the onshore and offshore wind farm cases with different turbine layouts, along with the TKE profile of the incoming boundary layer flows. In the present study, the normalized TKE is defined as

$$\mathrm{TKE} = \frac{1}{2} * \frac{\left(\overline{u'^2} + \overline{v'^2} + \overline{w'^2}\right)}{U_{\mathrm{Hub}}^2} \tag{2}$$

where u', v', and w' represent velocity fluctuations along the x, y, and z-axes, respectively. U_{Hub} is the streamwise velocity at hub height of the wind turbine.

As shown in Figure 6, in comparison with the turbulence levels of the incoming boundary flows, there is a strong enhancement in the TKE levels for the turbine wake flows in the regions around the top tip of turbine rotor for all the tested cases. The region corresponding to the maximum enhancement of the TKE intensity was found to be along the shedding path of the wake vortex structures generated by the upstream turbine blades, which agrees well with the particle image velocimetry measurement results in the turbine near wake as given in Hu et al.[6] In addition, as shown in Figure 6, the presence of the wind turbine was found to cause a decrease in the TKE levels in the turbine wakes for the regions below the turbine hub height, in comparison with that of the incoming boundary layer flows. Similar flow characteristics were also observed by Chamorro and Porté-Agel.[8] This can be explained by the fact that, in comparison with the incoming boundary layer flow, the turbulent mixing in the turbine wakes leads to a weaker shear layer in the regions near the ground as shown in Figure 4, which would reduce the TKE production in these regions.

Figure 7 gives the measured TKE profiles along the spanwise direction at the turbine hub height for the farms with different turbine layouts. Without the influence of wall effects near the ground, the turbine tower, and nonuniform inflow, the effects of wake vortices on the TKE levels were revealed clearly from the measured spanwise TKE profiles. As shown in Figure 7, the maximum enhancement of the TKE levels in the turbine wakes was found to be near the top of the turbine rotor blade tips, which was directly associated with the

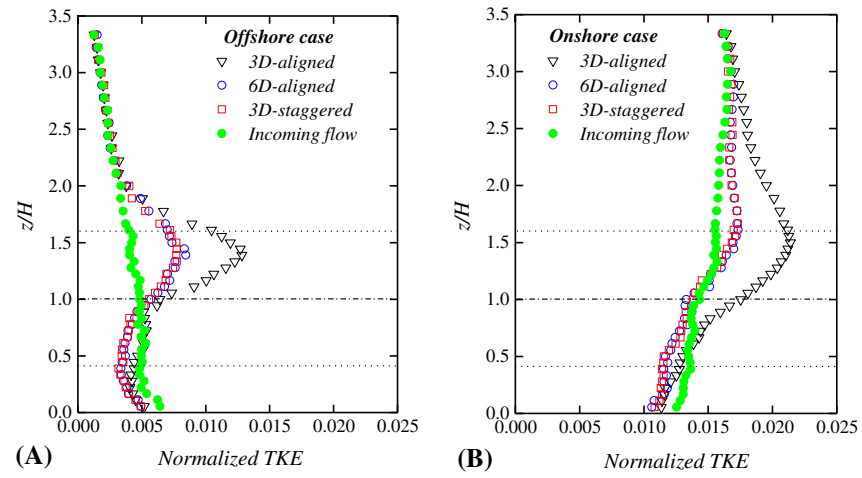

FIGURE 6 Measured turbulent kinetic energy (TKE) profiles along the vertical direction for the farms with different turbine layouts: A, offshore case; B, onshore case [Colour figure can be viewed at wileyonlinelibrary.com]

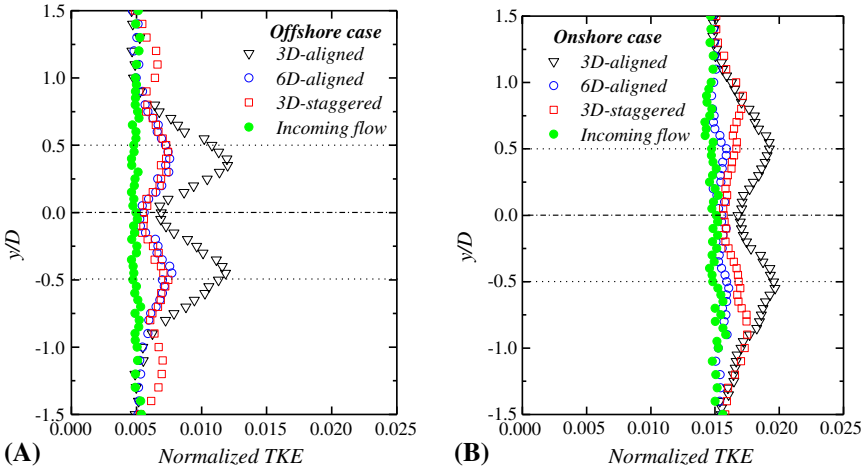

FIGURE 7 Measured turbulent kinetic energy (TKE) profiles along the spanwise direction for the farms with different turbine layouts: A, offshore case; B, onshore case [Colour figure can be viewed at wileyonlinelibrary.com]

shedding of the unsteady vortex structures from the upstream turbines. In addition, the enhancement of the TKE levels induced by the blade root vortices and flow separation behind the nacelle was found to be relatively low, in comparison with that in the region behind the tips of the rotor blades.

A significant difference in the TKE magnitudes between the offshore and onshore cases can be seen clearly based on the measurement results given in Figures 6 and 7. As suggested by Markfort et al,[20] the recovery rate of the velocity deficits in the turbine wakes would be closely related to the kinematic shear stresses and turbulence intensity levels in the turbine wakes. Vertical flux of the flow kinetic energy would be promoted by the high shear stresses and turbulence intensities over the wind farms, resulting in a faster extraction of high speed flows to recharge the low momentum flows inside the wind farms. Therefore, the higher turbulence levels for the onshore farm cases were found to cause a much faster recovery of the velocity deficits in the turbine wakes, as shown clearly in Figures 4 and 5.

Another difference can also be observed from the comparison of the TKE distributions between the offshore and onshore cases. As shown in Figure 7A, the TKE peaks were found to move inward slightly with respect to the positions of the blade tips for the offshore case. As described above, the appearance of TKE peaks believed to be closely related to the shedding of the wake vortices generated by the upstream turbines. As expected, after shed from the upstream turbines, the direct impact of the wake vortices onto the downstream turbines would lead to highly unsteady wind loads acting on the downstream turbine. However, for the onshore cases, as shown in Figure 7B, under the influence of high wake expansion associated with the high turbulence intensities in the incoming flow, the TKE peaks were found to move outward, instead of moving inward as those for the offshore cases. As a result, the effects of wake vortices generated by the upstream turbines on the dynamic wind loads experienced by the downstream wind turbine would become less significant for the onshore cases, in comparison with those of the offshore cases.

The spanwise TKE profiles given in Figure 7 can also be used to reveal the lateral shadowing effects of the staggered upstream turbines on the downstream turbines. As shown in Figure 7A, the presence of 2 turbines in the second row for the 3*D*-staggered layout was found to have almost no influence on the TKE distribution within the rotor region of the downstream turbine for the offshore case. It indicates that the shadowing effects of the upstream turbines on the downstream turbines can be greatly mitigated by using the 3*D*-staggered layout in offshore wind farms. However, for the onshore case, the high turbulence levels in the incoming flow would enhance the expansion of the turbine wake greatly. The wakes of the staggered upstream wind turbines would affect a much wider region in onshore wind farms, in comparison with those in offshore wind farms. As shown in Figure 7B, the TKE levels with the 3*D*-staggered layout were found to be higher than those with the 6*D*-aligned layout within the rotor region of the downstream turbine (ie, in the region of $-0.5 \le y/D \le 0.5D$). For the onshore case, the turbulent wake flow induced by the staggered turbines in the second row has expanded into the region where the downstream turbine was mounted, resulting in an additional TKE increase in the turbine wake. In comparison with the case with 6*D*-aligned layout, the additional TKE for the 3*D*-staggered layout would promote turbulent mixing in the wake flows, leading to a rapid recovery of the velocity deficits in the turbine wakes. Therefore, in comparison with the offshore case, the local flow acceleration caused by the lateral offset of the upstream staggered turbines was found to become more evident for the onshore case, which was also confirmed quantitatively from the measured velocity profiles given in Figure 5.

3.2 | Aeromechanical performance of the wind turbines

3.2.1 | Power output measurements of the wind turbine models

As described above, the power output data given in the present study correspond to the maximum power outputs of the model wind turbines, which were measured under the optimal TSR. The maximum power coefficient of the upstream wind turbines without any wake interferences for the offshore case was found to be 0.27 under the optimal TSR = 4.5, while this value was found to be 0.30 under the optimal TSR = 4.7 for

the onshore case. Because the focus in the present study is on the power losses caused by the wake interferences among the wind turbines placed in wind farms with different layouts, normalized power outputs (ie, normalized by the upstream undisturbed wind turbine) were adopted to evaluate the efficiency of the different wind farm layouts.

Figure 8 gives the normalized power outputs of the turbine models for the 3 compared layouts. The variations in the turbine power outputs can be explained reasonably based on the measured flow velocity profiles in the wind farms. For the offshore cases, the power outputs of the turbine models sited in the wind farms with 3*D*-staggered layout were found to be only slightly higher than those in 6*D*-aligned layout (ie, $C_p \approx 0.20$ for 3*D*-staggered layout and $C_p \approx 0.19$ for 6*D*-aligned layout), which is consistent with the measured flow velocity characteristics shown in Figures 4 and 5. In comparison with the 6*D*-aligned layout case, the slight increase in the turbine power output for the 3*D*-staggered layout case is believed to be caused by the Venturi effect induced by the upstream staggered wind turbines, which would enable the downstream wind turbine to extract more kinetic energy from the same incoming flow. The existence of similar positive venturi effects on power generation of dense wind turbine clusters was also reported in Ammara et al.[34] For the onshore cases, in addition to the Venturi effect, the much higher turbulence intensity in the incoming flow would also be helpful to promote the recovery of the turbine wake flows approaching the downstream turbine. Therefore, as shown clearly in Figure 8, the differences in the turbine power outputs for the 3*D*-staggered and 6*D*-aligned layouts were found to be more significant for the onshore cases, in comparison with the offshore cases.

It can also be seen that the power loss of the downstream turbine is much smaller when mounted in the wind farm with 3*D*-staggered layout, in comparison with that in the 3*D*-aligned layout, for both the offshore and onshore settings. As shown in Figure 8, the power outputs of the downstream turbines were found to be approximately 80% in the wind farms with 3*D*-staggered layout (ie, the power losses due to the turbine wake interferences was found to be ~20%). The finding was found to agree well with the field measurement data obtained in typical wind farms.[21,23,35] However, even though both the streamwise and spanwise turbine spacing in the 3*D*-aligned layout are the same as those in the 3*D*-staggered layout, the power losses of the downstream turbines in 3*D*-aligned layout were found to be much greater than those in 3*D*-staggered layout (ie, the power losses due to the turbine wake interferences were found to become greater than 45%). It is obvious that the 3*D*-aligned layout may not be a good choice for wind farm layout design due to the significant power losses for the downstream turbines caused by the wake interferences.

In comparison with those of the offshore cases, the higher inflow turbulence levels for the onshore cases would promote the turbulent mixing in the wind farm. As suggested by Tian et al,[11] the enhanced turbulence mixing in the turbine wakes for the onshore cases would augment the vertical flux of kinetic energy transport by extracting more high-speed flow (ie, high kinetic energy) from the airflow above the wind farms into the low momentum region inside the wind farms, thereby facilitating the recovery of the velocity deficits in the turbine wakes. As a result, the downstream wind turbines sited in onshore wind farms were found to experience much less power losses caused by the wake interferences from the upstream wind turbines. As shown clearly in Figure 8, with the same 3*D*-staggered layout for the wind farms, the power loss of the turbine model sited at the central position of the last row was found to be approximately 15% for the onshore case, which is only approximately half of that of the offshore case (ie, 27%).

3.2.2 | Dynamic wind loads

In addition to measuring the power outputs, the dynamic wind loads acting on the wind turbines are also important to consider for the optimum mechanical design of the turbines, as they can greatly affect the fatigue lifetimes of the wind turbines. In the present study, the wind loads acting on the model turbines were also examined to evaluate the effects of the inflow characteristics and the wind farm layouts on the dynamic wind loads acting on the wind turbines sited in the wind farms. The measured thrust coefficient C_T, bending moment coefficient C_{My}, lateral force coefficient C_y, and their standard deviations are listed in Table 1. The coefficients of the wind loads are all defined with respect to the inflow velocity at hub height (ie, U_{Hub}). As the comparison baselines, while the standard deviation of the thrust coefficient for the undisturbed upwind turbine was found

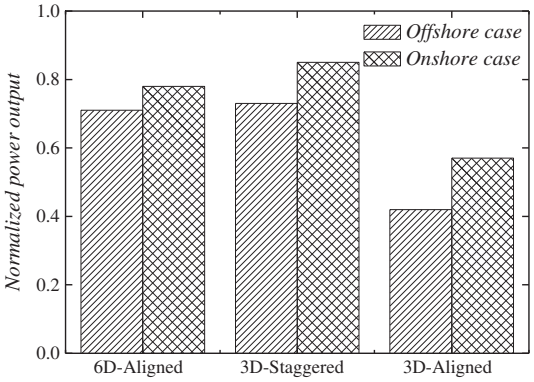

FIGURE 8 Normalized power outputs of the downstream turbines sited at the last row of the wind farms

TABLE 1 Dynamic wind loads acting on the central wind turbine in the last row of the wind farms

Wind Loads Acting on Central Wind Turbine Sited in Last Row of Wind Farm	Offshore Case			Onshore Case		
	6*D*-Aligned	3*D*-Staggered	3*D*-Aligned	6*D*-Aligned	3D-Staggered	3*D*-Aligned
Mean thrust coefficient, C_T	0.320	0.321	0.233	0.367	0.388	0.312
Standard deviation of thrust coefficient, σ_{CT}	0.145	0.145	0.222	0.190	0.201	0.277
Mean bending moment coefficient, C_{My}	0.357	0.360	0.256	0.412	0.433	0.348
Standard deviation of bending moment coefficient, σ_{CMy}	0.133	0.133	0.230	0.194	0.199	0.275
Mean lateral force coefficient, C_y	0.015	0.017	0.009	0.008	0.011	0.012
Standard deviation of lateral force coefficient, σ_{Cy}	0.101	0.104	0.104	0.144	0.155	0.153

to be σ_{CT} = 0.112 with the mean value of C_T = 0.411 for the offshore case, the standard deviation of the thrust coefficient was σ_{CT} = 0.165 with the mean value of C_T = 0.436 for onshore case.

It is interesting to note that, while the mean values of the wind loads acting on the tested turbine models sited in wind farms with different layouts were found to correlate well with the characteristics of the mean flow velocity profiles plotted in Figures 4 and 5, the variations in the standard deviations of the measured instantaneous wind loads were closely related to the measured TKE profiles given in Figures 6 and 7. For the offshore case (ie, with relatively low inflow turbulence levels), because the existence of the 2 staggered turbines in the second row was found to have almost no effects on the mean flow velocity and TKE profiles at the location where the downstream turbine was mounted, no distinct differences were observed in either the measured mean or fatigue loads between the test cases of the 6*D*-aligned and the 3*D*-staggered layouts. However, for the onshore case (ie, with much higher inflow turbulence levels), because wake expansion was greatly enhanced by the high turbulence levels, the downstream wind turbine sited in the wind farm with 3*D*-staggered layout would see a greater flow velocity and elevated TKE levels due to the effects of the 2 staggered upstream turbines, in comparison with the 6*D*-aligned layout case. Corresponding to the higher mean flow velocity approaching the turbine, the mean wind loads acting on the downstream turbine sited in the wind farm with 3*D*-staggered layout were found to be greater than those of the case with 6*D*-aligned layout. Corresponding to the elevated turbulence levels (ie, as indicated by higher TKE values) induced by the upstream turbines in the 3*D*-staggered onshore wind farm, the downstream wind turbine sited at the center of the third row of the 3*D*-staggered wind farm was found to experience greater fatigue loads, in comparison with those of the 6*D*-aligned layout case.

Because the wind speed seen by the downstream wind turbine mounted at the center of the last row for the 3*D*-aligned layout case is much lower than that of the 3*D*-staggered layout case, the mean wind loads acting on the downstream turbine sited in the 3*D*-aligned wind farms were found to be much smaller than those of the 3*D*-staggered layout for both the offshore and onshore cases. However, due to the much higher turbulence levels induced by the additional upstream turbines and much closer spacing between the turbine rows, the downstream turbines in the wind farms with 3*D*-aligned layout were found to experience higher fatigue loads than those of the 3*D*-staggered layout cases. For example, under the same offshore condition, the magnitude of the standard deviation of the thrust coefficients for the downstream turbine mounted at the center of the last row was found to be σ_{CT} = 0.222 for the 3*D*-aligned layout case, which is approximately 50% higher than that of the 3*D*-staggered layout case (ie, σ_{CT} = 0.145).

Because the incoming boundary layer flow is symmetric about the center line of the wind farm, the mean values of the lateral force coefficients, C_y, for the tested wind turbines were found to be always very small and can be neglected in comparison with the other wind loading components. However, as listed in Table 1, the fluctuation amplitudes of the lateral forces were found to be very significant; ie, the standard deviation values of the lateral force coefficients were found to be almost at the same level as those of the thrust coefficients. The quantitative measurement results presented here highlight the fact that the fluctuations of the lateral forces acting on the wind turbines should also be considered properly in the turbine mechanical design. For the onshore cases, the lateral shadowing effects of the upstream staggered turbines on the downstream turbines can also be observed from the measured standard deviations of the lateral force coefficients listed in Table 1. More specifically, the presence of the upstream staggered turbines was found to cause the standard deviation values of the lateral force coefficients for the downstream turbine to increase from σ_{Cy} = 0.144 to σ_{Cy} = 0.155 (ie, ~8% increase) due to the turbine wake expansion in the spanwise direction.

In the present study, the power spectra of the measured instantaneous wind loads were also obtained via a fast Fourier transform procedure, and the results are given in Figure 9. The dominant peaks observed in the power spectrum plots correspond to the rotation frequency of the turbine rotor blades (ie, the turbine rotation frequency f_o). The rotation frequencies of turbine rotor blades identified based on the fast Fourier transform analysis were found to agree well with those measured independently by using a tachometer.

As shown in Figure 9, for the offshore cases, well-defined dominant peaks (ie, the peaks at the frequency f_o) can be observed clearly for all the 3 compared layout cases. However, for the onshore cases with much higher turbulence levels for the incoming flows, the rotational frequencies of the turbines were found to fluctuate greatly in a wide frequency range, and a group of peaks (ie, the peaks around the frequency f_o) can be observed in the power spectrum plots. As indicated by Tian et al,[11] the significant fluctuations in the rotational frequencies of the turbine blades for the onshore cases would suggest higher fluctuations of the wind loads (ie, greater fatigue loads) acting on the wind turbines when they are sited in onshore wind farms. It was also revealed clearly that the spectrum plots for the 3*D*-staggered layout cases (ie, both for onshore of offshore cases) are quite similar to those of the 6*D*-aligned cases. It suggests that the 2 staggered turbines sited in the second row of the 3*D*-staggered layout farm have almost no significant influence on the dynamic wind loads acting on the downstream turbine. It can also be seen that, for the offshore cases

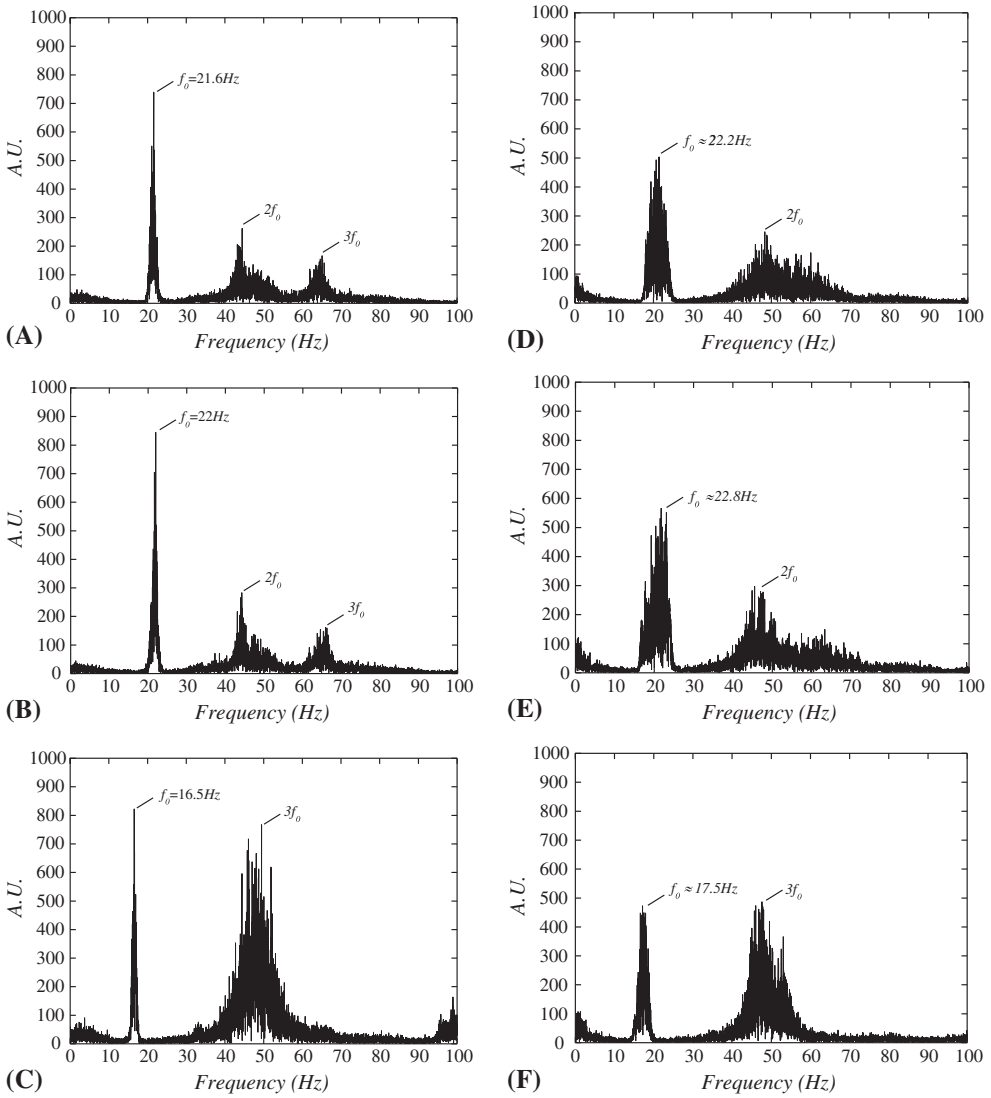

FIGURE 9 Power spectrum of the measured instantaneous thrust acting on the turbine model sited in the wind farms with different layouts. A, 6*D*-aligned, offshore case; B, 3*D*-staggered, offshore case; C, 3*D*-aligned, offshore case; D, 6*D*-aligned, onshore case; E, 3*D*-staggered, onshore case; F, 3*D*-aligned, onshore case

with relatively low inflow turbulence levels, in addition to the peaks corresponding to the rotation frequency of the turbine blades f_0, other peaks, which represent the harmonic frequencies of the turbine rotation frequency (ie, $2f_o$ and $3f_o$ peaks), can be identified clearly in the plots.

However, for the onshore cases with higher inflow turbulence levels, because the turbine rotation frequencies were found to fluctuate greatly in wide frequency ranges, the harmonic frequencies of the turbine rotation frequency, especially for $3f_o$ peaks, become almost indistinguishable in the power spectrum plots for the 6*D*-aligned and 3*D*-staggered layout cases. It is worth noting that, in comparison with the power spectrum plot of the instantaneous wind loads acting on an isolated wind turbine presented in Tian *el al*,[11] the power spectrum plots for the 6*D*-aligned and 3*D*-staggered layout cases shown in Figure 9A and B were found to have very similar characteristics (ie, very similar defined peaks at turbine rotation frequency f_0 and the harmonic frequencies $2f_o$ and $3f_o$). It implies that the upstream turbine wakes have almost no distinct effects on the dynamic characteristics of the wind loads acting on downstream wind turbines for the offshore cases.

As shown in Figure 9C and F, the power spectrum plots for the 3*D*-aligned layout case show very different features, in comparison with those of the 6*D*-aligned and 3*D*-staggered layout cases. While the harmonic frequencies of $2f_o$ become almost in indistinguishable in the power spectrum plots, the peaks around $3f_o$ were found to be in a much wider region for both the offshore and onshore cases. Such feature changes revealed in the power spectrum plots are believed to closely related to the more complicated wake interferences and interactions of the wake vortices shed from the upstream turbines of the 3*D*-aligned layout case. As described above, due to the small spacing between the upstream and downstream turbines in the 3*D*-aligned wind farms, the wake vortices shedding from the upstream turbines do not have enough distance to break down and dissipate in the 3*D*-aligned wind farms. The superimposed turbine wakes from the upstream multiple turbines would cause much more complex incoming flow conditions for the downstream turbines sited in the last row of the 3*D*-aligned wind farm. The more complex incoming turbulent flows, which were the superimposed turbine wakes with different wake vortex structures at various scales and frequencies, would lead to highly fluctuating wind

loads (ie, greater fatigue loads) acting on the downstream turbines. Therefore, distinct wide regions of the peaks around $3f_o$ are revealed in the power spectrum plots for the 3*D*-aligned layout cases.

3.3 | Efficiencies of the wind farms with aligned and staggered layouts

In addition to investigating the aeromechanical performances of the downstream turbines sited in the wind farms with different turbine layouts, the overall farm efficiency was also examined in the present study to evaluate the effects of the inflow characteristics and the turbine layout designs on the overall power production capacity of the wind farms. In the present study, the overall farm efficiency of a wind farm is defined based on the following equation:

$$\eta = \frac{P_{\text{Total}}}{\sum P_{\text{individual}}} = \frac{\sum_{i=1}^{n} P_i}{\sum_{i=1}^{n} P_{\text{individual},i}} \tag{3}$$

where $P_{\text{individual},i}$ is the power generation of an individual turbine exposed to the undisturbed inflows (ie, without any turbine wake interferences), P_{Total} is the overall power output produced by all the model turbines sited in the wind farm, and n is the number of wind turbines in the wind farm. To determine $P_{\text{individual},i}$, a turbine model was mounted at various positions defined by the wind farm layout without the presence of any other wind turbines. P_{Total} was determined by summing up all the power outputs of the model turbine sited at various locations defined by the wind farm layout along with all the other wind turbines present in the wind farm (ie, with the effects of the wake interferences from the upstream turbines).

Figure 10 gives the measured overall farm efficiency for all the studied wind farms with different turbine layout designs. It should be noted, while the measurement results given in Figure 10 were found to show quite similar trend as those given in Figure 8, the physical meaning of the plots is quite different. While the measurement results given in Figure 8 are based on the measured power output of a single downstream turbine sited in the center position at the last row of a wind farm, the measured overall farm efficiency data given in Figure 10 represent the overall power production performance of the wind farm with the power outputs of all the wind turbines in the wind farm being considered. For a specific wind farm design, because the power losses due to the wake interferences induced by the upstream turbines would be more significant for the downstream turbines, the normalized power output data given in Figure 8 were found to be much smaller than the corresponding values of the overall farm efficiency given in Figure 10, as expected.

As shown in Figure 3B, because there are no upstream turbines for the 2 staggered turbines at the second row of the 3*D*-staggered layout, the 2 turbines were exposed to the same undisturbed incoming flow as that of the turbines at the first row. As a result, no power losses due to the wake interferences would occur for the 2 turbines sited in the second row, which leads to a higher farm efficiency for the 3*D*-staggered wind farm, in comparison with the 6*D*-aligned layout case. For the 3*D*-staggered onshore farm design, both the lateral offset of the upstream turbines and the higher inflow turbulence levels would help to enhance the turbulent mixing in the wind farm for a faster recovery of the velocity deficits in the turbine wake flows. Therefore, the 3*D*-staggered onshore farm case was found to have the highest overall farm efficiency among all the compared cases. While the overall farm efficiency for the 3*D*-staggered layout design was found to be 94% for the onshore case, the corresponding value for the 6*D*-aligned layout case was approximately 88%. The differences between the 6*D*-aligned and 3*D*-staggered layout cases were found to become less pronounced for the offshore cases, in comparison with those of the onshore cases.

It can also be seen that the overall farm efficiencies for the 3*D*-aligned wind farm design were found to be only approximately 64% and 67% for the offshore and onshore cases, respectively. The values are much lower than those of the 3*D*-staggered layout case even though the 2 layout designs have the same streamwise and spanwise turbine spacing. The comparison of the overall farm efficiency between the 3*D*-aligned and 3*D*-staggered layout designs highlights again the importance of the turbine layout in the optimization design of a wind farm because it can influence the power generation of the wind farm significantly. It can also be found that, for the 3*D*-aligned wind farm design, the difference of the overall farm efficiencies between the offshore and onshore cases (ie, 64% and 67%) shown in Figure 10 is much smaller than that of the measured power outputs of the single downstream wind turbine (ie, 41% and 58%) given in Figure 8. As shown in Figures 4 and 5, the effects of inflow turbulence on

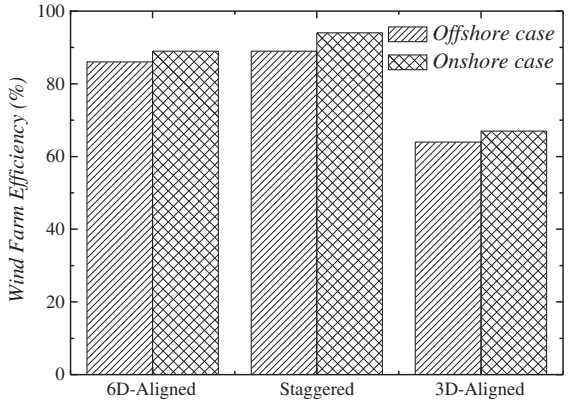

FIGURE 10 Overall farm efficiency of the studied wind farms with different turbine layout designs

the wake flow were found to become increasingly obvious as the downstream distance increases. Therefore, the differences in the turbine wakes between the onshore and offshore cases would be much smaller at the downstream locations of the second row turbines for the 3*D*-aligned layout (ie, 3*D* away from the upstream undisturbed turbines), in comparison with those of the third row turbines (ie, 6*D* away from the upstream undisturbed turbines). As a result, the power outputs of the wind turbines sited in the second row of the 3*D*-aligned wind farm for the onshore case were found to be only slightly higher than those of the offshore case, lessening the difference between the offshore and onshore cases in the term of overall farm efficiency.

4 | CONCLUSION

An experimental investigation was performed to examine the effects of the incoming flow characteristics and turbine layout patterns on the wake interferences among multiple wind turbines sited in wind farms. The experimental study was performed in a large-scale ABL wind tunnel available at Iowa State University. Two different types of boundary layer flows with distinct mean and turbulence characteristics were generated in the wind tunnel to simulate the different inflow characteristics cover typical onshore and offshore wind farms. An array of wind turbine models was mounted inside the boundary layer flows to form small wind farms with different layout pattern and turbine spacing (ie, 3*D*-staggered layout vs 3*D*-aligned layout vs 6*D*-aligned layout). During the experiments, in addition to quantifying the characteristics of the turbine wake flows inside the wind farms, the aeromechanic performances of the turbine models, including power outputs and dynamic wind loads, were also evaluated under different inflow conditions. The effects of the farm layout designs on the power production efficiency of the wind farm were also examined based on the quantitative measurement results.

It was found that both the incoming flow characteristics and wind farm layouts would affect the turbine wake interferences and aeromechanic performances of the wind turbines dramatically. The power outputs of the wind turbines sited in a wind farm were found to be closely related to the characteristics of wake interferences within the wind farm. For the 3*D*-staggered layout, the 2 laterally offset wind turbines sited in the second row were found to have a beneficial effect on promoting the velocity deficit recovery of the turbine wake flows as they approach the downstream turbines. As a result, the downstream wind turbines sited in the third row of the 3*D*-staggered layout were found to be able to extract more kinetic energy from the same incoming boundary layer flows, in comparison with those in the wind farms with other 2 compared layout designs (ie, 3*D*-aligned or 6*D*-aligned layout designs). The flow acceleration induced by the upstream staggered turbines was found to be more significant for the onshore case (ie, the case with higher turbulence levels in the incoming flow) than to that of the offshore case (ie, the case with relatively low turbulence levels in the incoming flow).

While the mean wind loads acting on the model turbines were correlated well with the time-averaged velocity profiles of the turbulent flows at the turbine mounting sites, the fatigue loads (ie, the standard deviations of the measured instantaneous wind loads) experienced by the tested turbines were found to be closely related to the TKE characteristics of the turbulent flows approaching the wind turbines. For the offshore case, because the effects of the wake expansion from the 2 staggered turbines sited in the second row of the 3*D*-staggered layout could not reach the regions where the downstream turbines were mounted, the fatigue loads acting on the downstream turbines in the 3*D*-staggered layout were found to be very similar to those in the wind farm with 6*D*-aligned layout. However, for the onshore case, with much higher turbulence levels in the incoming flow, the turbulent flow structures induced by the upstream wind turbines were found to expand into a much wider region. With the effects of the enhanced turbulence levels induced by the 2 staggered wind turbines in the second row, the downstream wind turbines sited in the third row of the 3*D*-staggered layout were found to experience higher fatigue loads than those in the 6*D*-aligned layout.

For the 3*D*-aligned layout case, due to the smaller turbine spacing, the wake vortices shedding from the upstream turbines do not have enough distance to break down and dissipate. The superimposed turbine wakes from the upstream turbines would make the wake flows much more complex as they approaching the downstream wind turbines in the third row of the 3*D*-aligned layout. The complex wake flows, which include multiple vortex structures with various scales and frequencies shed from the upstream turbine, were found to result in much greater fatigue loads acting on the downstream wind turbines sited in the 3*D*-aligned layout, in comparison with those with 3*D*-staggered and 6*D*-aligned layouts.

It should also be noted that the turbine layouts investigated in the present study represent only the first 2 or 3 rows of a wind farm. As noted by Chamorro et al,[19] the turbine wake flow in a large wind farm can be divided into a developing region and a developed region. The turbine wake flows would develop and reach an equilibrium state after a certain number of rows. The focus of the present study is on the developing region of a wind farm, where the turbine wake flows have not yet reached the equilibrium state. More extensive researches are still needed to quantify the characteristics of the turbine wake flows and to evaluate their effects on the aeromechanic performances of wind turbines in the developed region of a wind farm.

ACKNOWLEDGEMENTS

The authors want to thank the funding support from the National Science Foundation (NSF) with grant numbers CBET-1133751 and CBET-1438099 and the Iowa Energy Center with grant number 14-008-OG. Wei Tian also wants to thank the support from the National Key Technology Support Program of China (no 2015BAA06B04) and the Shanghai Natural Science Foundation (no 16ZR1417600).

ORCID

Wei Tian http://orcid.org/0000-0001-5038-0492

REFERENCES

1. Barthelmie RJ, Folkerts L, Ormel F, et al. Offshore wind turbine wakes measured by SODAR. *J Atmos Oceanic Tech*. 2003;20:466-477.
2. Corten G, Schaak P, Hegberg T. Turbine interaction in large offshore wind farms: wind tunnel measurements. Netherlands Agency for Energy and Environment, paper ECN-C-04-048, 2004.
3. Adaramola M, Krogstad P. Experimental investigation of wake effects on wind turbine performance. *Renew Energy*. 2011;36:2078-2086.
4. Sanderse B. Aerodynamics of wind turbine wakes: literature review. Energy Research Center of the Netherlands, paper ECN-E-09-016, 2009.
5. Wu Y, Porte-Agel F. Large-eddy simulation of wind-turbine wakes: evaluation of turbine parametrizations. *Bound-Lay Meteorol*. 2010;138:345-366.
6. Hu H, Yang Z, Sarkar P. Dynamic wind loadings and wake characteristics of a wind turbine model in an atmospheric boundary layer wind. *Experiments in Fluids*. 2012;52:1277-1294.
7. Zhang W, Markfort CD, Porte-Agel F. Near-wake flow structure downwind of a wind turbine in a turbulent boundary layer. *Experiments in Fluids*. 2012;52:1219-1235.
8. Chamorro L, Porte-Agel F. A wind-tunnel investigation of wind-turbine wakes: boundary-layer turbulence effects. *Bound-Lay Meteorol*. 2009;132:129-149.
9. Wu Y, Porté-Agel F. Atmospheric turbulence effects on wind-turbine wakes: an LES study. *Energies*. 2012;5:5340-5362.
10. Chu CR, Chiang PH. Turbulence effects on the wake flow and power production of a horizontal-axis wind turbine. *Journal of Wind Engineering and Industrial Aerodynamics*. 2014;124:82-89.
11. Tian W, Ozbay A, Hu H. Effects of incoming surface wind conditions on the wake characteristics and dynamic wind loadings acting on a wind turbine model. *Phys Fluids*. 2014;26: 125108
12. Sescu A, Meneveau C. Large-eddy simulation and single-column modeling of thermally stratified wind turbine arrays for fully developed, stationary atmospheric conditions. *J Atmos Oceanic Tech*. 2015;32:1144-1162.
13. Wu Y, Porté-Agel F. Modeling turbine wakes and power losses within a wind farm using LES: an application to the Horns Rev offshore wind farm. *Renew Energy*. 2015;75:945-955.
14. Yang X, Sotiropoulos F, Conzemius RJ, Wachtler JN, Strong MB. Large-eddy simulation of turbulent flow past wind turbines/farms: the Virtual Wind Simulator (VWiS). *Wind Energy*. 2015;18:2025-2045.
15. Cortina G, Calaf M, Cal RB. Distribution of mean kinetic energy around an isolated wind turbine and a characteristic wind turbine of a very large wind farm. *Physical Review Fluids*. 2016;1: 074402
16. Crespo A, Hernaandez J, Frandsen S. Survey of modelling methods for wind turbine wakes and wind farms. *Wind Energy*. 1999;2:1-24.
17. Cal RB, Lebrón J, Castillo L, Kang HS, Meneveau C. Experimental study of the horizontally averaged flow structure in a model wind-turbine array boundary layer. *Journal of Renewable and Sustainable Energy*. 2010;2: 013106
18. Chamorro LP, Porte-Agel F. Turbulent flow inside and above a wind farm: a wind-tunnel study. *Energies*. 2011;4:1916-1936.
19. Chamorro LP, Arndt R, Sotiropoulos F. Turbulent flow properties around a staggered wind farm. *Bound-Lay Meteorol*. 2011;141:349-367.
20. Markfort CD, Zhang W, Porté-Agel F. Turbulent flow and scalar transport through and over aligned and staggered wind farms. *Journal of Turbulence*. 2012;33:1-36.
21. Barthelmie RJ, Hansen K, Frandsen S, et al. Modelling and measuring flow and wind turbine wakes in large wind farms offshore. *Wind Energy*. 2009;12:431-444.
22. Frandsen S, Antoniou I, Hansen J, et al. Redefinition power curve for more accurate performance assessment of wind farms. *Wind Energy*. 2000;3:81-111.
23. Barthelmie RJ, Pryor SC, Frandsen ST, et al. Quantifying the impact of wind turbine wakes on power output at offshore wind farms. *J Atmos Oceanic Tech*. 2010;27:1302-1317.
24. Hansen KS, Barthelmie RJ, Jensen LE, Sommer A. The impact of turbulence intensity and atmospheric stability on power deficits due to wind turbine wakes at Horns Rev wind farm. *Wind Energy*. 2012;15:183-196.
25. Annoni J, Howard K, Seiler P, Guala M. An experimental investigation on the effect of individual turbine control on wind farm dynamics. *Wind Energy*. 2016;19:1453-1467.
26. Theunissen R, Housley P, Allen CB, Carey C. Experimental verication of computational predictions in power generation variation with layout of offshore wind farms. *Wind Energy*. 2015;18:1739-1757.
27. Bossuyt J, Howland MF, Meneveau C, Meyers J. Measurement of unsteady loading and power output variability in a micro wind farm model in a wind tunnel. *Experiments in Fluids*. 2017;58:1
28. Bossuyt J, Meneveau C, Meyers J. Wind farm power fluctuations and spatial sampling of turbulent boundary layers. *J Fluid Mech*. 2017;823:329-344.
29. Australian Standard. Minimum design loads on structures (known as the SAA loading code). AS 1170.2-1989.
30. Locke J, Valencia U. Design studies for twist-coupled wind turbine blades. Sandia National Laboratories, Technical Report No. SAND 2004-0522, 2004.
31. Somers DM. The S819, S820, and S821 Airfoils. National Renewable Energy Laboratory, Technical Report No. NREL/SR-500-36334, 2005.
32. Ozbay A, Tian W, Hu H. An experimental investigation on the wake characteristics and aeromechanics of dual-rotor wind turbines. *ASME Journal of Engineering for Gas Turbines and Power*. 2016;138: 042602
33. Kang HS, Meneveau C. Direct mechanical torque sensor for model wind turbines. *Measurement Science & Technology*. 2010;21:105206

34. Ammara I, Leclerc C, Masson C. A viscous three-dimensional differential/actuator-disk method for the aerodynamic analysis of wind farms. *Journal of Solar Energy Engineering*. 2002;124:345-356.

35. Storm B, Dudhia J, Basu S, Swift A, Giammanco I. Evaluation of the weather research and forecasting model on forecasting low-level jets: implications for wind energy. *Wind Energy*. 2009;12:81-90.

How to cite this article: Tian W, Ozbay A, Hu H. An experimental investigation on the wake interferences among wind turbines sited in aligned and staggered wind farms. *Wind Energy*. 2018;21:100–114. https://doi.org/10.1002/we.2147